

Spontaneous symmetry breaking and vortices in a tri-core nonlinear fractional waveguide

Mateus C. P. dos Santos,^{1,*} Wesley B. Cardoso,¹

Dmitry V. Strunin,² and Boris A. Malomed^{3,4}

¹*Instituto de Física, Universidade Federal de Goiás, 74.690-900, Goiânia, Goiás, Brazil*

²*School of Mathematics, Physics and Computing,
University of Southern Queensland, Toowoomba, Queensland 4350, Australia*

³*Department of Physical Electronics, School of Electrical Engineering,
Faculty of Engineering, and the Center for Light-Matter Interaction,
Tel Aviv University, P.O.B. 39040, Ramat Aviv, Tel Aviv, Israel*

⁴*Instituto de Alta Investigación, Universidad de Tarapacá, Casilla 7D, Arica, Chile*

Abstract

We introduce a waveguiding system composed of three linearly-coupled fractional waveguides, with a triangular (prismatic) transverse structure. It may be realized as a tri-core nonlinear optical fiber with fractional group-velocity dispersion (GVD), or, possibly, as a system of coupled Gross–Pitaevskii equations for a set of three tunnel-coupled cigar-shaped traps filled by a Bose-Einstein condensate of particles moving by Lévy flights. The analysis is focused on the phenomenon of spontaneous symmetry breaking (SSB) between components of triple solitons, and the formation and stability of vortex modes. In the self-focusing regime, we identify symmetric and asymmetric soliton states, whose structure and stability are determined by the Lévy index of the fractional GVD, the inter-core coupling strength, and the total energy, which determines the system’s nonlinearity. Bifurcation diagrams (of the supercritical type) reveal regions where SSB occurs, identifying the respective symmetric and asymmetric ground-state soliton modes. In agreement with the general principle of the SSB theory, the solitons with broken inter-component symmetry prevail with the increase of the energy in the weakly-coupled system. Three-components vortex solitons (which do not feature SSB) are studied too. Because the fractional GVD breaks the system’s Galilean invariance, we also address mobility of the vortex solitons, by applying a boost to them.

* mateuscalixtopereira@gmail

I. INTRODUCTION

Nonlinear Schrödinger (NLS) equations are a set of universal models governing the wave propagation in dispersive nonlinear media [1, 2], such as optical fibers [3], bulk media and photonic crystals [4], Langmuir waves in plasmas [5, 6], matter waves Bose-Einstein condensates (BECs) [7, 8], magnetics [9], surface waves in fluids [10, 11] and solids [12], etc. Commonly known solutions of the NLS equations are fundamental solitons and higher-order ones (breathers [13]), which have been created experimentally in a great variety of physical setups.

A natural extension of the single NLS equation is a system of linearly coupled ones, which describe copropagation of nonlinear waves in tunnel-coupled channels, a well-known example being dual-core [14–17] and tri-core [18, 19] optical fibers. Recently, much interest was drawn to nonlinear optics in multi-core fibers, that support various multi-mode propagation regimes [20–23].

Nonlinear dual-core systems support obvious states in the form of two-component solitons which are symmetric with respect to the coupled cores. An effect induced by the intra-core self-focusing nonlinearity in dual-core systems is the spontaneous symmetry breaking (SSB). It occurs above a critical value of the soliton's energy, when the symmetric solitons with equal components lose their stability and are replaced by asymmetric ones with unequal components. This effect was studied in detail theoretically [16, 17], and recently demonstrated experimentally in dual-core optical fibers [24].

A somewhat similar realization of soliton SSB was studied in models based on a single NLS equation with the cubic self-focusing nonlinearity concentrated at two mutually symmetric points in the form of delta-functions [25, 26], as well as in their two-component version [27]. In those models, SSB was realized as spontaneous establishment of a stationary structure in the form of two mutually asymmetric spikes with unequal amplitudes, pinned to the two delta-functions.

Another novel direction for the study of NLS-like solitons is focused on the fractional NLS (FNLS) equations. They were originally derived, in the linear form, by dint of the Feynman-integral formalism as quantum-mechanical equations for particles moving by Lévy flights in the classical limit [28–31]. While such a quantum-mechanical setting has not been yet realized experimentally, it was later proposed to implement essentially the

same linear equations as classical ones for the propagation of optical beams in the paraxial approximation, emulating the effect of the fractional diffraction by a phase shift introduced for different spectral components by means of a properly designed phase plate [32]. The optical realization of the fractional linear Schrödinger equation in the temporal domain, i.e., in a fiber cavity, has been reported in Ref. [33], where the phase shifts emulating the action of the fractional group-velocity dispersion (FGVD) was created as a computer-generated hologram.

The possibility to implement the fractional diffraction/dispersion in optics suggests one to include the nonlinearity of the dielectric material, the respective model being naturally based on FNLS equations. This possibility has been elaborated theoretically in great detail. The predicted effects include modulational instability of continuous waves [34], many varieties of quasi-linear modes [35, 36] and solitons [35–41], including gap solitons in optical lattices [42, 43], multipole and multipole modes [44–48], soliton clusters [49, 50], PT-symmetric solitons [79, 80], and solitary vortices [50, 51]. Reviews of the theoretical results for solitons in models based on FNLS and related equations are offered by Refs. [52] and [53].

The SSB effect for two-component solitons in fractional dual-core couplers has also been addressed [54–56]. The next natural step is to consider a tri-core linearly-coupled system with the combination of FGVD and cubic self-focusing acting in each core, which is modeled by a system of three coupled FNLS equations (note that the experimental realization of FGVD, reported in Ref. [33] for single-core fiber cavities, can be readily implemented for multi-core systems as well). This is the subject of the present work. The system of coupled equations is introduced in Section II, which is followed by the analysis of the SSB phenomenology and families of three-component solitons in this system, reported in Section III. Vortex solitons, with winding number 1 carried by the triangular (prismatic) set of three complex components (cf. Ref. [57]), are considered in Section IV, where their stability area is identified, and it is found that the vortex solitons do not give rise to SSB, i.e., they are extremely robust modes. In the same section, mobility of vortex solitons is addressed too, by means of systematic simulations. The paper is concluded by Section V.

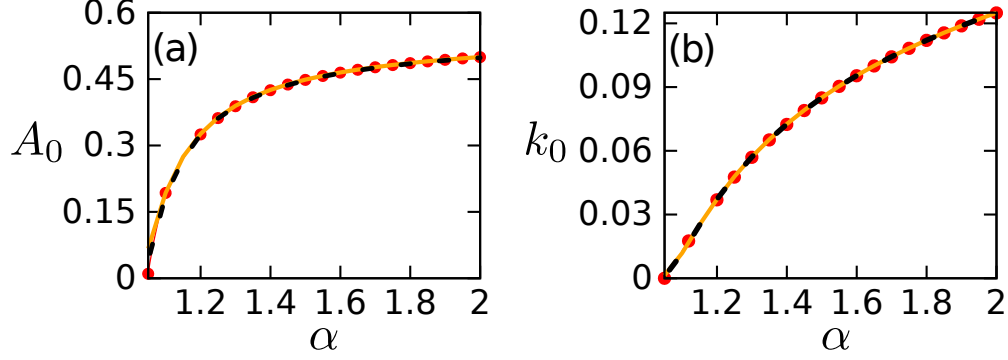


FIG. 1: Coefficients A_0 (a) and k_0 (b) from Eqs. (11) and (12) versus α . The results, as obtained from numerically found ground-states (GS) solutions of Eq. (8) for different energies, $E = 1, 1.3$ and 1.5 , are displayed by solid lines (orange), dotted lines (black) and circles (red), respectively. The identical equality of these coefficients for all values of E corroborates the validity of scaling relations (11) and (12).

II. THE MODEL

A. Three linearity coupled fractional nonlinear Schrödinger (FNLS) equations

We consider the model of the tri-core optical fiber with the triangular (prismatic) cross-section structure and amplitudes $U_{1,2,3}(t, z)$ of the optical waves propagating in the three linearly-coupled cores with the FGVD and Kerr self-focusing nonlinearity carried by each core. In the scaled form, the corresponding system of the coupled FNLS equations takes the form (cf. similar systems for the tri-core fibers with the regular (non-fractional) dispersion [18, 32]):

$$\begin{aligned}
 i\frac{\partial U_1}{\partial z} &= \frac{1}{2} \left(-\frac{\partial^2}{\partial t^2} \right)^{\alpha/2} U_1 - |U_1|^2 U_1 - \lambda (U_2 + U_3), \\
 i\frac{\partial U_2}{\partial z} &= \frac{1}{2} \left(-\frac{\partial^2}{\partial t^2} \right)^{\alpha/2} U_2 - |U_2|^2 U_2 - \lambda (U_3 + U_1), \\
 i\frac{\partial U_3}{\partial z} &= \frac{1}{2} \left(-\frac{\partial^2}{\partial t^2} \right)^{\alpha/2} U_3 - |U_3|^2 U_3 - \lambda (U_1 + U_2).
 \end{aligned} \tag{1}$$

Here the evolutional variable z is, as usual [3] the propagation distance, t is the temporal coordinate, and $\lambda > 0$ is the coupling constant. By means of rescaling, the Kerr-

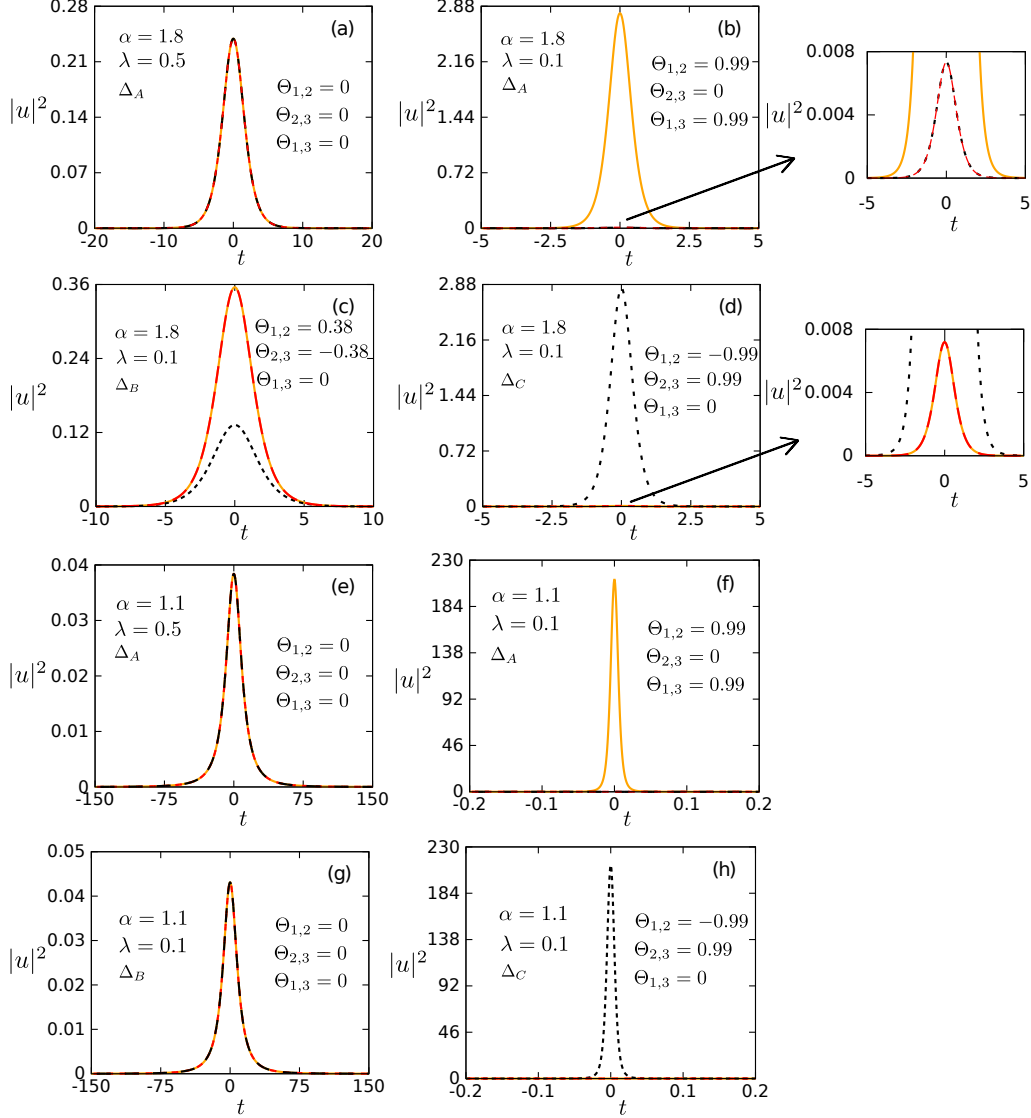


FIG. 2: Symmetric and asymmetric GS (ground-state) solitons in the three-core system with total energy $E = 3$ are shown by means of their power profiles, $|u_1(t)|^2$, $|u_2(t)|^2$, and $|u_3(t)|^2$, which are plotted by orange solid lines, black dotted lines, and red dashed lines, respectively. They were obtained by the imaginary-time simulations of Eq. (1) from the inputs (13a), (13b), and (13c), as indicated by symbols $\Delta_{A,B,C}$ in each panel (values of LI α and linear-coupling coefficient λ are also indicated in the panels). The solitons in panels (a, b) and (d-h) are stable, while the one in panel (c) is unstable. The asymmetric solitons in panels (b) and (d) exhibit bistability, belonging to the coexistence region shown in Fig. 8(a). The solitons in panels (f-h) realize a tristability case, belonging to the highlighted region of Fig. 9(a).

nonlinearity and FGVD coefficients in Eqs. (1) are fixed to be +1 or -1 (the signs of the coefficients imply cubic self-focusing and anomalous dispersion [3]). FGVD is represented by the fractional Riesz derivative [58], which is a pseudo-differential (actually, integral) operator, defined as the juxtaposition of the direct and inverse Fourier transforms,

$$\left(-\partial^2/\partial t^2\right)^{\alpha/2} U = \frac{1}{2\pi} \int_{-\infty}^{+\infty} d\omega |\omega|^\alpha \int_{-\infty}^{+\infty} d\tau e^{-i\omega(\tau-t)} U(\tau), \quad (2)$$

with the Lévy index (LI) α [59], which takes values $1 < \alpha \leq 2$. With regard to the definition (2), the Hamiltonian of system (1) can be written as

$$\begin{aligned} H = \sum_{j=1,2,3} \left[\frac{1}{2\pi} \int_0^\infty \omega^\alpha d\omega \int_{-\infty}^{+\infty} dt \int_{-\infty}^{+\infty} d\tau \cos(\omega(t-\tau)) \right. \\ \left. \times U_j^*(\tau) U_j(t) - \frac{1}{2} \int_{-\infty}^{+\infty} dt |U_j(t)|^4 \right] \\ - \lambda \int_{-\infty}^{+\infty} dt \sum_{j \neq k} U_j^*(t) U_k(t), \end{aligned} \quad (3)$$

where * stands for the complex conjugate.

The classical (non-fractional) derivative corresponds to $\alpha = 2$. Smaller values, $\alpha \leq 1$ give rise to the wave collapse in the FNLS equation, which makes all solitons unstable [39]).

One may conjecture that the same system (1), with z replaced by scaled time, and t replaced by a scaled coordinate, may appear as Gross-Pitaevskii equations for mean-field wave functions of the BEC of quantum particles that are governed, at the individual level, by the fractional linear Schrödinger equation, in the case when the BEC is loaded into a tunnel-coupled set of parallel cigar-shaped potential traps that form a triangular (prismatic) structure, cf. Ref. [60]. However, a consistent derivation of such fractional Gross-Pitaevskii equations was not reported, as yet.

Non-topological (zero-vorticity) soliton solutions to Eq. (1) with real propagation constant k are looked for as

$$U_{1,2,3}(t, z) = e^{ikz} u_{1,2,3}(t), \quad (4)$$

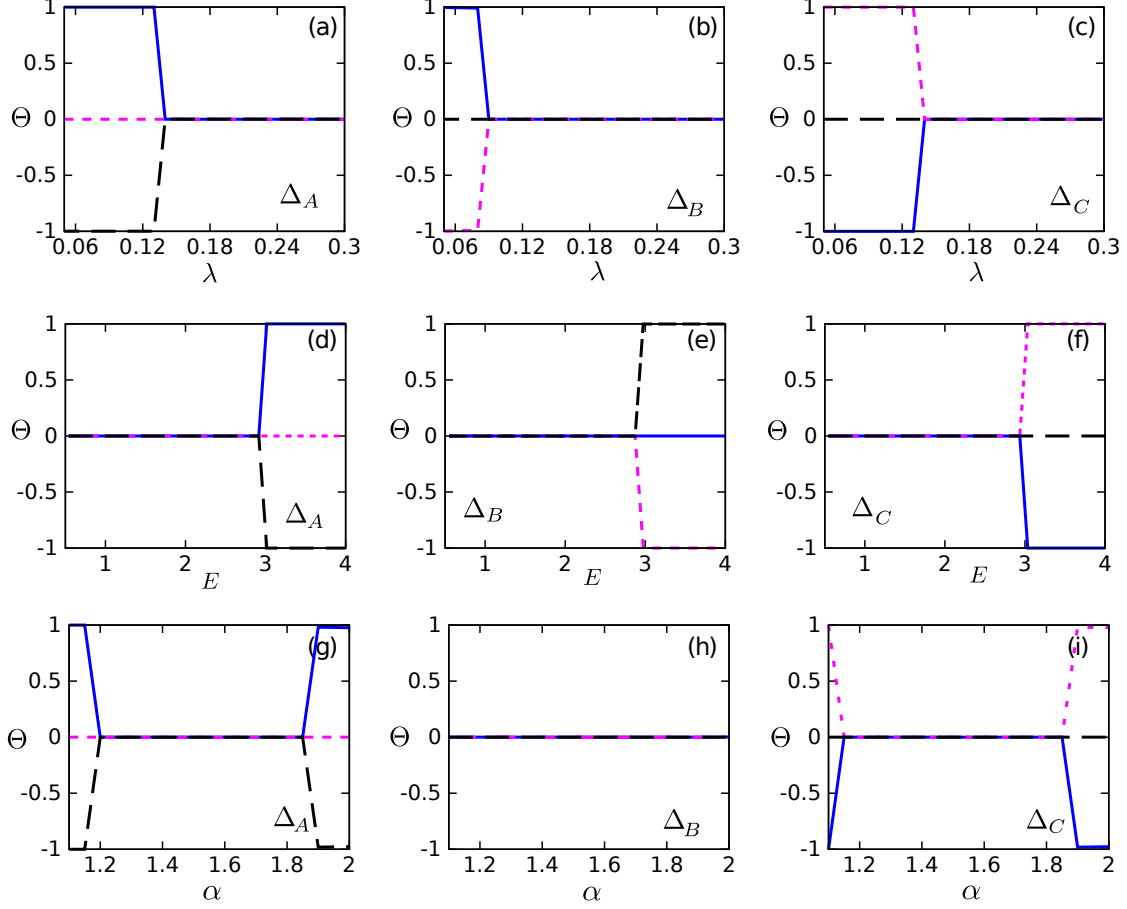


FIG. 3: Asymmetry ratios (7) Θ plotted versus λ , E and α , for the GS solitons by the different inputs of types Δ_A , Δ_B and Δ_C (see Eq. (13a) - (13c)). The results for $\Theta_{1,2}$, $\Theta_{2,3}$ and $\Theta_{3,1}$ are displayed by solid (blue), dotted (magenta) and dashed (black) lines, respectively. The other parameters are: (a-c) $\alpha = 1.1$ and $E = 3$; (d-f) $\alpha = 1.1$ and $\lambda = 0.13$; and (g-i) $E = 3$ and $\lambda = 0.13$.

where $u_{1,2,3}(t)$ must be real localized solutions of the system of three coupled equations:

$$\begin{aligned}
 ku_1 + \frac{1}{2} \left(-\frac{d^2}{dt^2} \right)^{\alpha/2} u_1 - u_1^3 - \lambda (u_2 + u_3) &= 0, \\
 ku_2 + \frac{1}{2} \left(-\frac{d^2}{dt^2} \right)^{\alpha/2} u_2 - u_2^3 - \lambda (u_3 + u_1) &= 0, \\
 ku_3 + \frac{1}{2} \left(-\frac{d^2}{dt^2} \right)^{\alpha/2} u_3 - u_3^3 - \lambda (u_1 + u_2) &= 0.
 \end{aligned} \tag{5}$$

It is expected that the system (5) admits more than a single species of asymmetric solitons, as a result of SSB, cf. Ref. [19], where a similar problem was considered for a triangular set of linearly-coupled Bragg gratings (with the usual first-order derivatives, instead of

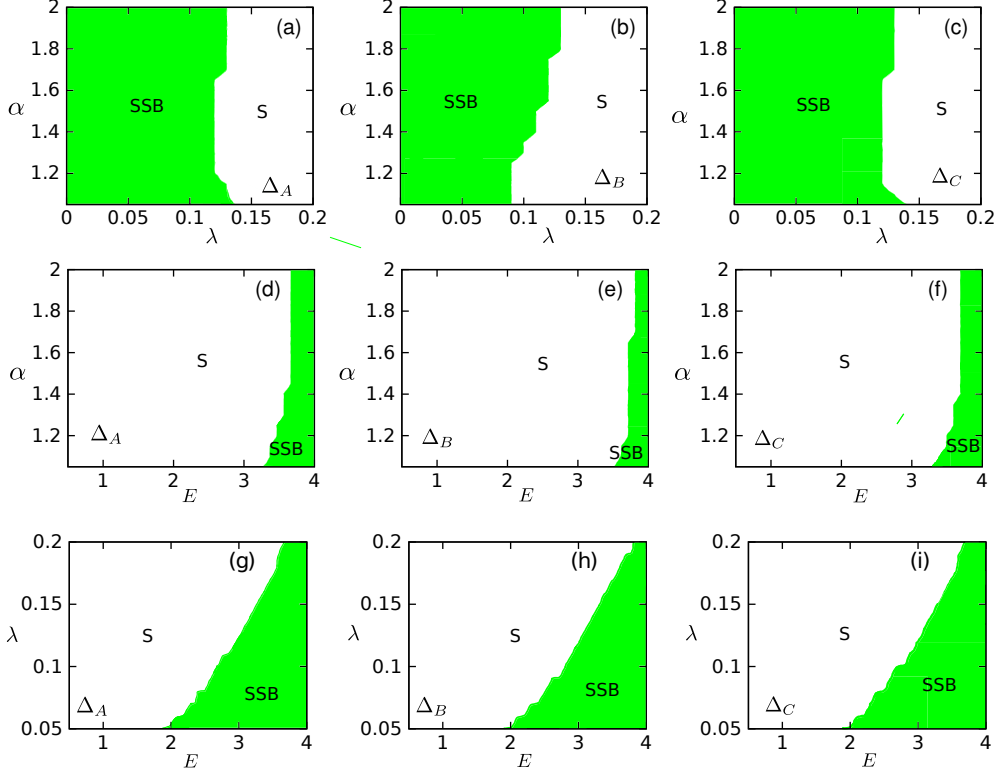


FIG. 4: Phase diagrams for (a)symmetric solitons produced by inputs of types Δ_A , Δ_B and Δ_C , see Eqs. (13a), (13b), and (13c). The S (white) and SSB (green) areas are populated by stable symmetric and asymmetric GS solitons, respectively. The parameters used here are: (a-c) $E = 3$; (d-f) $\lambda = 0.2$, and (g-i) $\alpha = 1.7$.

the second-order ones or their fractional counterparts).

Soliton solutions of Eq. (5) are characterized by their total energy (norm),

$$E = \sum_{j=1,2,3} E_j \equiv \sum_{j=1,2,3} \int_{-\infty}^{+\infty} |U_j|^2 dt, \quad (6)$$

where E_j is the energy carried by each core. In the present conservative system, E is a dynamically invariant of Eq. (1), while partial energies E_j are not, as the cores can exchange the energy through the linear coupling.

The structure of solutions with unequal components u_j produced by system (5) is characterized by the set of *asymmetry ratios*,

$$\Theta_{n,m} = \frac{E_n - E_m}{E_n + E_m}, \quad (7)$$

which are defined as relative difference in the energies of the optical fields in different cores. These SSB parameters take values $-1 \leq \Theta_{n,m} \leq +1$. Symmetric solitons with

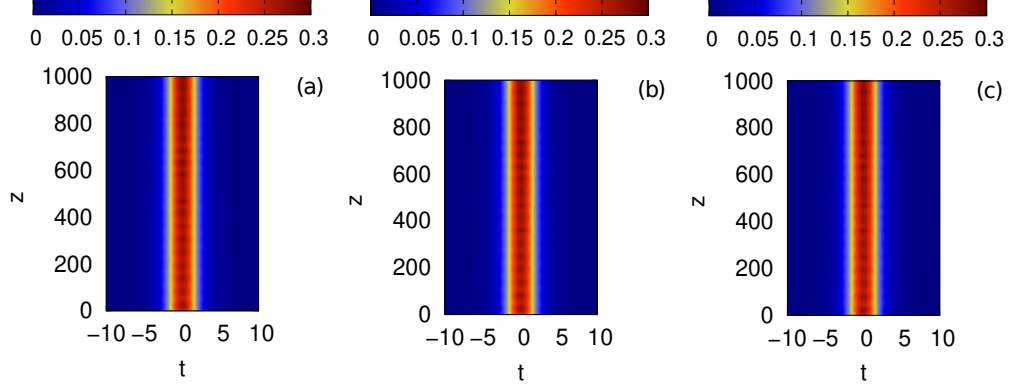


FIG. 5: The perturbed evolution of components $|U_1|^2$, $|U_2|^2$ and $|U_3|^2$ of a stable symmetric soliton with $\alpha = 1.6$, $\lambda = 0.5$ and $E = 3$, is displayed in panels (a), (b) and (c), respectively. The profiles were initially perturbed according to Eq. (15).

equal energies in all cores have, obviously, $\Theta_{n,m} = 0$ for all pairs of indices (m, n) . On the other hand, limit values $\Theta_{n,m} = 1$ or $\Theta_{n,m} = -1$ indicate that the core m or n is empty, carrying no energy.

Thus, while the asymmetry parameter of the usual double-core couplers is a scalar, it is a three-component vector in the case of the three-core system, which makes the results quite different, as shown below.

B. Scaling for single-component fractional solitons

The single stationary FNLS equation, which corresponds to the decoupled system(5) with $\lambda = 0$, i.e.,

$$ku + \frac{1}{2} \left(-\frac{d^2}{dt^2} \right)^{\alpha/2} u - u^3 = 0. \quad (8)$$

gives rise to known scaling relations for its soliton solutions [52, 53]. Namely, varying k leads to the following *exact* relations between k , the soliton's amplitude A and its width W :

$$k \sim W^{-\alpha} \sim A^2. \quad (9)$$

Accordingly, the energy of the single-component soliton, $E = \int_{-\infty}^{+\infty} u^2(t) dt$, scales as $E \sim A^2 W$, i.e., $W \sim E/A^2$. The substitution of this expression for W in Eq. (9) leads to the following exact relation between A^2 and E :

$$A \sim E^{\alpha/2(\alpha-1)}. \quad (10)$$

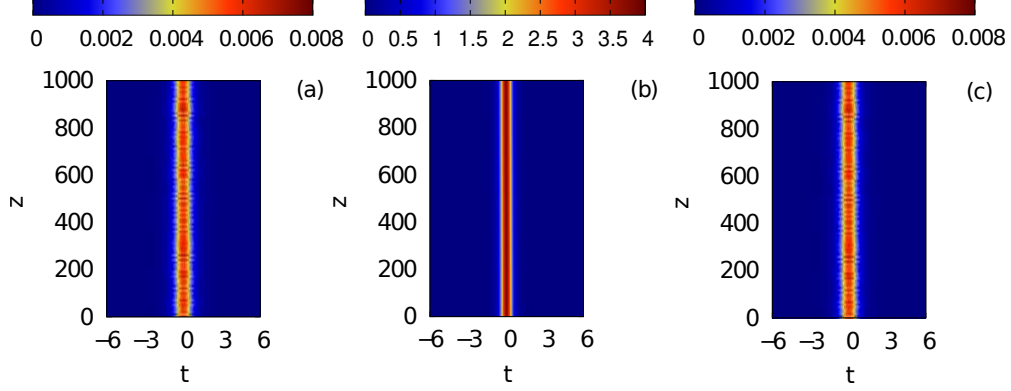


FIG. 6: The perturbed evolution of components $|U_1|^2$, $|U_2|^2$ and $|U_3|^2$ of a stable asymmetric soliton for $\alpha = 1.7$, $\lambda = 0.1$, $E = 3$ and input Δ_C , is displayed in panels (a), (b) and (c) respectively.

In a detailed form, Eq. (10) can be rewritten as

$$A = A_0(\alpha)E^{\alpha/2(\alpha-1)}, \quad (11)$$

where coefficient $A_0(\alpha)$ may be a function of LI α , but not of E .

In addition to that, it follows from Eqs. (10) and (9) that k and E are related by the following scaling,

$$k = k_0(\alpha)E^{\alpha/(\alpha-1)}. \quad (12)$$

The limit values of coefficients A_0 and k_0 in Eqs. (11) and (12) are $A_0(\alpha = 2) = 1/2$ and $k_0(\alpha = 2) = 1/8$ (see Fig. 1), which correspond to the classical soliton solutions of the non-fractional NLS equation, with $\alpha = 2$. On the other hand, the singularity of relations (11) and (12) in the limit of $\alpha = 1$ implies that the limit values of the coefficients are $A_0(\alpha \rightarrow 1), k_0(\alpha \rightarrow 1) \rightarrow 0$.

To illustrate these relations, in Fig. 1 we display three different curves of A_0 and k_0 versus α . The results were obtained as numerically found ground-states of Eq. (8) for $E = 1.0, 1.3$ and 1.5 , which identically coincide, in agreement with Eqs. (11) and (12). Thus, coefficients $A_0(\alpha)$ and $k_0(\alpha)$ are universal characteristics of the solitons produced by the single FNLS equation.

III. SPONTANEOUS SYMMETRY BREAKING (SSB) IN THREE-COMPONENT GROUND-STATE (GS) SOLITONS

Numerical simulations of the system (1) were performed by dint of the imaginary- and real-time propagation algorithms based on the Fourier spectral method [66]. The imaginary-time simulations were used, as usual [67], to construct stationary soliton solutions that represent the system's ground state (GS), which minimizes the Hamiltonian (3) for given total energy (6). Note that the symmetry of the underlying three-core system implies that GSs represented by asymmetric solitons are degenerate, as mutually equivalent GSs can be obtained from each other by cyclic transpositions of subscripts 1, 2, 3, cf. Refs. [62, 68–70]. Then, the real-time simulations were employed to test stability of the solitons and study their dynamical properties.

The imaginary-time simulations were initiated from the set of Gaussian inputs $U_j(t, z = 0) = B_j \exp(-t^2)$, with $j = 1, 2$ and 3 . The corresponding amplitudes B_j 's were obtained to produce three initial conditions following small values of asymmetries (7):

$$\Delta_A \equiv \begin{cases} \Theta_{1,2} = 0.01, \\ \Theta_{2,3} = 0.01, \\ \Theta_{1,3} = 0.02, \end{cases} \quad (13a)$$

$$\Delta_B \equiv \begin{cases} \Theta_{1,2} = 0.01, \\ \Theta_{2,3} = -0.01, \\ \Theta_{1,3} = 0, \end{cases} \quad (13b)$$

$$\Delta_C \equiv \begin{cases} \Theta_{1,2} = -0.01, \\ \Theta_{2,3} = 0.01, \\ \Theta_{1,3} = 0. \end{cases} \quad (13c)$$

As shown below, these initial conditions can produce GS solitons with strong asymmetry.

In Fig. 2 we present generic examples of GS solitons. In particular, panels 2(a) and 2(b) displays the profiles obtained with two different values of λ , for LI $\alpha = 1.8$ and total power $E = 3$. Naturally, the GS soliton in panel 2(a), supported by relatively strong linear coupling, with $\lambda = 0.5$, is symmetric, while the one in panel 2(b), with much weaker linear coupling ($\lambda = 0.1$) is strongly asymmetric.

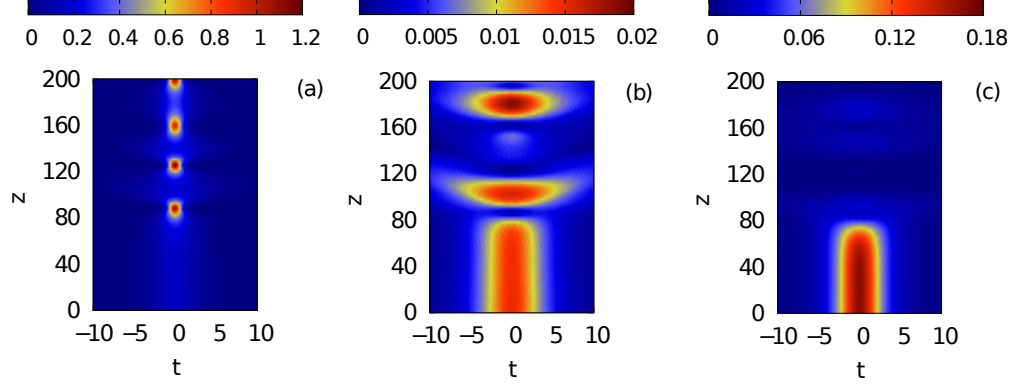


FIG. 7: The perturbed evolution of components $|U_1|^2$, $|U_2|^2$ and $|U_3|^2$ of an unstable asymmetric soliton, with $\alpha = 1.5$, $\lambda = 0.02$, $E = 2$ and input Δ_B , are displayed in the panels (a), (b) and (c), respectively.

Further, to elucidate the effect of the initial asymmetry, Figs. 2(b-d) present asymmetric GS solitons obtained from different inputs (13a)-(13c), keeping the same values of α , λ and E . The configurations displayed in these figures are drastically different, despite being obtained with the same parameters. In Fig. 2(b), input Δ_A produces identical (mutually symmetric) profiles $|u_2|^2$ and $|u_3|^2$, while $|u_1|^2$ is different. Accordingly, in this case the asymmetry is characterized by the combination

$$E_2 = E_3 < E_1, \quad (14)$$

with the amplitudes of u_2 and u_3 which are much smaller than that of u_1 , see the insert in Fig. 2(b).

The GS soliton resulting in Fig. 2(d) from the input of type Δ_C (Eq. (13c)) is asymmetric too, but subject to relation $E_1 = E_3 < E_2$, opposite to the one in Eq. (14). The input of type Δ_A (see Eq. (13a)) with the same values of the system's parameters produces the same GS soliton as in Fig. 2(d), but with $u_1 \longleftrightarrow u_2$. The GS solitons the tri-core system with $\alpha = 2$ (the usual non-fractional GVD) are similar to those produced here with $\alpha = 1.8$ (Figs. 2(a-d)), with the same symmetry and stability properties.

The GS solitons change abruptly under the action of FGVD, with smaller values of LI, such as $\alpha = 1.1$ (recall that all solitons are destabilized by the collapse in the case of $\alpha \leq 1$). For instance, Fig. 2(e) displays a fully symmetric GS soliton. In this case, the symmetric profiles are wide, in comparison to the case of larger LI, cf. Fig. 2(a). As

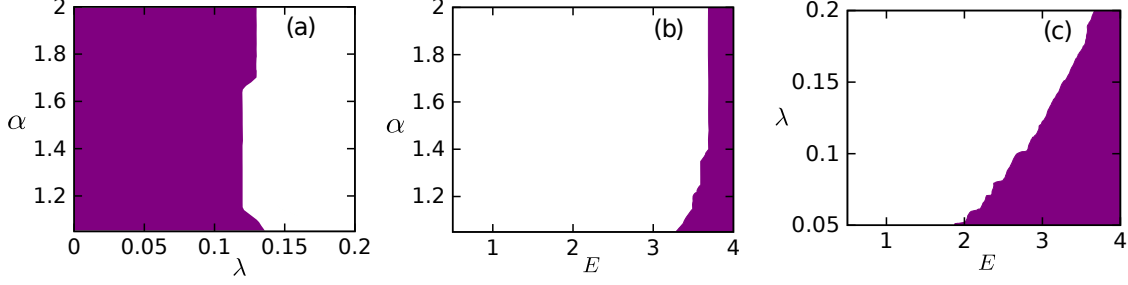


FIG. 8: Colored areas display bistability areas, in which stable asymmetric solitons, produced by the inputs of types Δ_A and Δ_C (see Eqs. (13a) and (13c)) coexist in the parameter planes plotted here. Other parameters are fixed as in Fig. 4.

concerns asymmetric GS solitons, they concentrate their energy in a single component, in agreement with the asymmetry of the input. In particular, the inputs of types Δ_A and Δ_C produce, respectively, GS solitons in which virtually all energy is concentrated in component u_1 or u_2 , as can be seen in Figs. 2(f) and (h). Another characteristic feature of the low-LI regime is a possibility of having a stable symmetric profile in the case of weak linear coupling ($\lambda = 0.1$), see Fig. 2(g).

In Fig. 3 we summarize the results for the GS soliton families by means of plots for the asymmetry ratios (7) versus the linear-coupling constant λ , total energy E , and LI α , obtained from the same inputs labeled by symbols Δ_A , Δ_B and Δ_C according to Eqs. (13a)-(13c). Here we focus the analysis on the configurations obtained with low LI values, i.e., ones are that most different from those produced by the usual (non-fractional) system, with $\alpha \rightarrow 2$. Fig. 3(a) demonstrates abrupt change in Θ following the decrease of λ , while E and α are fixed. Thus we observe that only asymmetric configurations are found in the regime of weak linear coupling, for $\lambda \leq 0.13$. In Fig. 3(b) where the input of the Δ_B type is used, the transition from asymmetric configurations to the symmetric ones (the SSB bifurcation point) is occurs at a still smaller value of the coupling constant, $\lambda = 0.08$. The curves $\Theta(\lambda)$ obtained with input Δ_C demonstrate, in Fig. 3(c), an abrupt transition, as in Fig. 3(a). However, in this configuration u_2 has higher energy than u_1 , producing $\Theta_{1,2} < 0$. Note that, the bifurcation point on the $\Theta(\lambda)$ curves are the same, indicating that the type of the input does not effect the SSB bifurcation.

To explore the effect of the total energy E , curves $\Theta(E)$ for the different inputs are plotted in Figs. 3(d-f). It is observed that, like in other SSB systems [17], the total energy

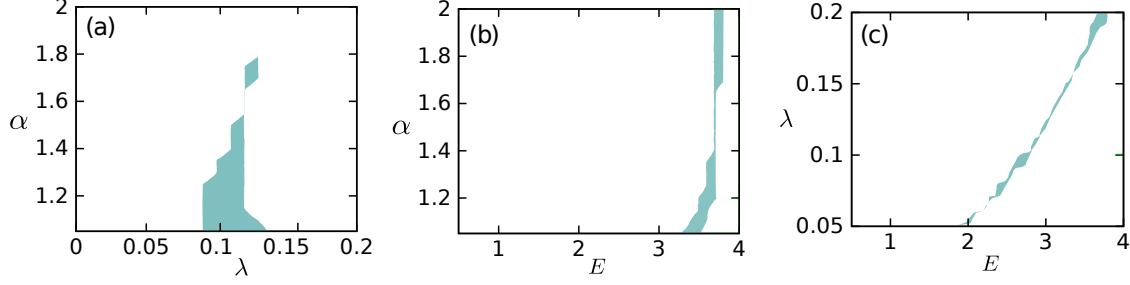


FIG. 9: Colored areas display tristability areas, in which two stable asymmetric solitons and a stable symmetric one, produced by the inputs of types Δ_A , Δ_C and Δ_B , respectively (see Eqs. (13a) - (13c)) coexist in the parameter planes plotted here. Other parameters are fixed as in Fig. 4.

controls the SSB in the present system too. The onset of SSB at the bifurcation point, exhibited by Figs. 3(d-f), identifies the bifurcation as one of the *supercritical* type (alias the symmetry-breaking phase transition of the second kind [71]), which implies that the symmetric states are destabilized by the bifurcation, while the asymmetric ones emerge as stable states, no bistability between symmetric and asymmetric solutions taking place.

Completely novel results, that demonstrate the asymmetry ratios as functions of LI, are presented in Figs. 3(g-i). In particular, a novel finding, reported in Figs. 3(g) and (i), is that curves $\Theta_{1,2}(\alpha)$ and $\Theta_{1,3}(\alpha)$ demonstrate two distinct regions of asymmetry, separated by broad symmetry interval, for the GS solitons produced by inputs Δ_A and Δ_C . On the other hand, input Δ_B produces solely fully symmetric states, as shown in Fig. 3(h).

To further summarize the findings, we have identified existence regions for different states, in the relation to parameters λ , E and α . In Fig. 4(a) we address the GS solitons obtained with $E = 3$ from input of type Δ_A , varying LI α and the linear-coupling constant λ . In general, the plot in the (λ, α) plane shows that the asymmetric states are naturally favored in the region of weak linear coupling. In Figs. 4(b) and (c), the same results are displayed, but now with the use of input Δ_B or Δ_C . In the former case, the SSB area is somewhat larger.

In Figs. 4(d-f), we address the effect of the total energy on the GS solitons at different values of LI, while fixing the coupling parameter as $\lambda = 0.2$. The resulting diagrams show that, as might be expected, the asymmetric states dominate at higher energies (i.e.,

stronger self-focusing nonlinearity), and are weakly favored by the decrease of LI. As in the previous cases, the diagram corresponding to input Δ_B is slightly different (see Fig. 4(b)) from those corresponding to Δ_A and Δ_C .

Finally, in Fig. 4(g-i) we investigated the combined effect of the coupling strength, λ , and total energy, E , on the GS solitons, fixing LI as $\alpha = 1.7$. Naturally, the symmetric GS is stabilized by the increase of λ and destabilized by the increase of E .

We tested the stability of GS solitons in direct real-time simulations, using the perturbed input

$$u_{1,2,3}(t, z = 0) = [1 + r_{1,2,3}(t)]u_{1,2,3}^{\text{GS}}(t, z = 0), \quad (15)$$

where $u_{1,2,3}^{\text{GS}}(t, z = 0)$ is the GS soliton obtained by the imaginary-time propagation, and $r_{1,2,3}(t)$ is a random function produced by the *rand* function of the *GNU-Octave* software, that perturbs the initial condition. Here, the maximum of the random perturbation corresponds to $\pm 3\%$ of the unperturbed soliton's amplitude, i.e., the random function takes values $-0.03 \leq r_{1,2,3}(t) \leq 0.03$ with mean value $\langle r_{1,2,3}(t) \rangle \simeq 0$. Using this protocol, we tested the stability of the GS solitons obtained above.

Symmetric soliton exhibit dynamic stability in the tests. In Fig. 5, we illustrate this conclusion by displaying the evolution of profiles $|U_{1,2,3}(t, z)|^2$ of a perturbed symmetric solitons obtained for $\alpha = 1.6$, $\lambda = 0.5$ and $E = 3$.

The tests of the evolution of the asymmetric solitons reveal stable and unstable ones. Further, the simulations demonstrate that, generally, the asymmetry solitons are more sensitive to disturbances. We conclude that the asymmetric solitons produced by the inputs of types Δ_A and Δ_C (see Eqs. (13a) and (13c)) demonstrate stability. As an example, in Fig. 6 we present the perturbed evolution of the asymmetric profiles obtained with $\alpha = 1.7$, $\lambda = 0.1$, $E = 3$ and Δ_C . The profiles $|U_1|^2$ and $|U_3|^2$ exhibit variations, but the soliton as a whole keeps its integrity, as shown by the fact that the evolution asymmetry ratios $\Theta(z)$ keep constant values (not shown here in detail).

On the contrary to what is shown above, the perturbed evolution of the asymmetric soliton generated by input Δ_B (see Eq. (13b)) demonstrates that the solitons of this type are completely unstable. In this case, the initial disturbance in Eq. (15) is enough to initiate apparent onset of instability, eventually leading to decay of the soliton (delocalization of the wave fields). As an example, we show in Fig. 7 the unstable perturbed evolution of an asymmetric soliton obtained with $\alpha = 1.5$, $\lambda = 0.02$ and $E = 2$. The shapes of the three

components start to change abruptly at $z \sim 50$. In particular, the profile $|U_1(t, z)|^2$, which had amplitude 0.17 at $z = 0$, quickly increases its value to 1.1 at $z = 88$. After this stage, the amplitude of $|U_1|^2$ decreases, performing quasi-periodic oscillations. Simultaneously, component U_2 presents slower oscillations, and U_3 suffers complete decay, showing the remaining energy $E_3 = 0.014$ at $z = 120$.

Figs. 2(b) and 2(d) demonstrate the coexistence of two different asymmetric solutions obtained with the same system's parameters α and λ , and equal energies E . These profiles, generated by different inputs, of types Δ_A and Δ_C (see Eqs. (13a) and (13c)), are stable, indicating the phenomenon of bistability. The coexistence regions of different stable asymmetric profiles are shown in Fig. 8. We also investigated the tristability, coexistence of three different types of stable solitons (tristability), *viz.*, two asymmetric ones and a symmetric soliton, also found for the same parameters. An example of this is provided a trio of solitons shown in Figs. 2(f-h). Fig. 9 displays parameter areas where the tristability is found in the planes of (λ, α) , (E, α) and (E, λ) .

	Initial condition of asymmetry	λ_c ($\alpha = 1.6$ and $E = 3$)	E_c ($\alpha = 1.6$ and $\lambda = 0.13$)
Weak	Δ_A ($\Theta_{12} = 0.01, \Theta_{23} = 0.01, \Theta_{13} = 0.02$)	0.13	2.9
	Δ_B ($\Theta_{12} = 0.01, \Theta_{23} = -0.01, \Theta_{13} = 0$)	0.12	2.9
	Δ_C ($\Theta_{12} = -0.01, \Theta_{23} = 0.01, \Theta_{13} = 0$)	0.13	2.9
Strong	$\Delta_{A'}$ ($\Theta_{12} = 0.2, \Theta_{23} = 0.4, \Theta_{13} = 0.6$)	0.24	2.3
	$\Delta_{B'}$ ($\Theta_{12} = 1, \Theta_{23} = -1, \Theta_{13} = 0$)	0.12	3.1
	$\Delta_{C'}$ ($\Theta_{12} = -0.99, \Theta_{23} = 0.99, \Theta_{13} = 0$)	0.36	1.9

TABLE I: Comparison between the critical values of interaction λ_c and energy E_c , obtained with weak (Δ_A, Δ_B and Δ_C) and strong ($\Delta'_{A'}, \Delta'_{B'}$ and $\Delta'_{C'}$) initial asymmetry conditions. The critical values define the onset of the SSB region.

The above analysis is focused on slightly asymmetric initial conditions (13a)-(13c), aiming to minimize the effect of the input's asymmetry and highlight the role of the inner evolution governed by system (1). Extensive simulations, conducted for various degrees of asymmetry of the initial conditions, produce similar results for GS solitons. Nevertheless, SSB regions may differ, depending on the degree of the initial asymmetry. To investigate this feature, we analyzed the shapes of the GS solitons obtained for three

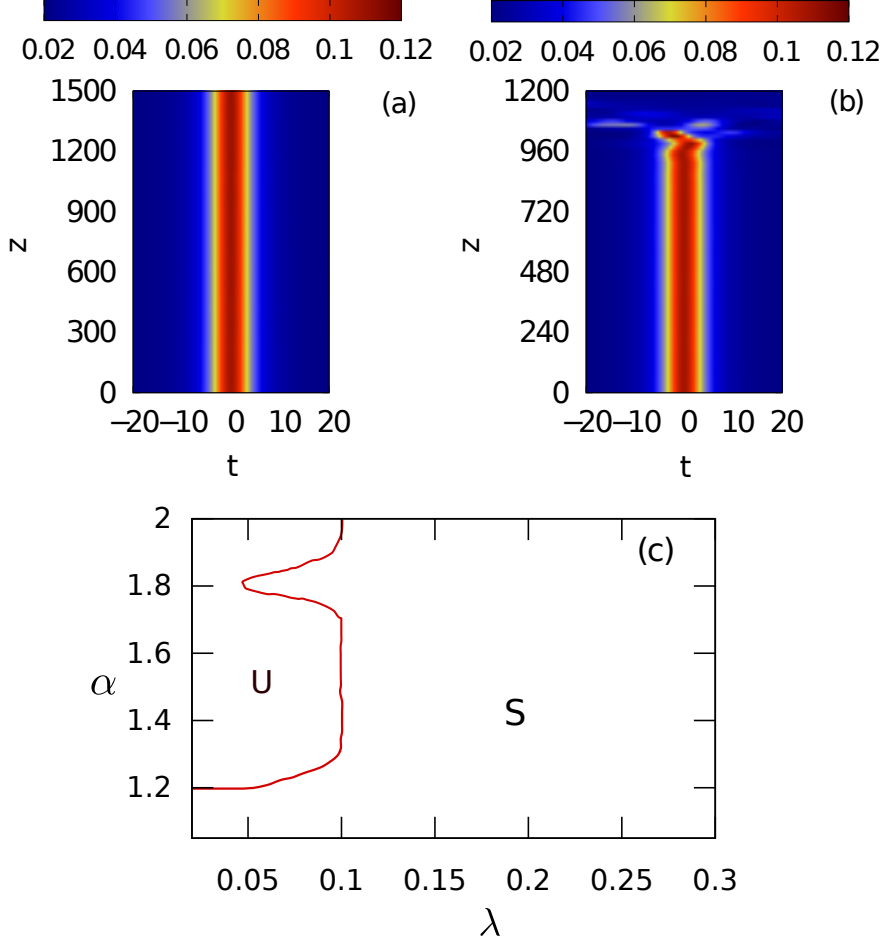


FIG. 10: The evolution of the component $|U_3|^2$ of an (un)stable vortex soliton (16) for $\alpha = 1.2$ and $\lambda = 0.1$ (a) or $\lambda = 0.05$ (b), as produced by simulations of Eq. (1). The total energy of the vortex soliton is $E = 3$. The evolution of other components, U_1 and U_2 , is similar. (c) The stability diagram for the vortex solitons with $E = 3$. They are stable and unstable in areas S and U, respectively.

strong asymmetric inputs, *viz.*, $\Delta_{A'} \equiv \Theta_{12} = 0.2$, $\Theta_{23} = 0.4$, $\Theta_{13} = 0.6$; $\Delta_{B'} \equiv \Theta_{12} = 1$, $\Theta_{23} = -1$, $\Theta_{13} = 0$; and $\Delta_{C'} \equiv \Theta_{12} = -0.99$, $\Theta_{23} = 0.99$, $\Theta_{13} = 0$, cf. Eqs. (13a)-(13c). The respective findings are compared to those obtained from the weakly asymmetry inputs (Δ_A , Δ_B and Δ_C), as given by Eqs. (13a)-(13c). Table I summarizes the respective results, presenting the corresponding critical values of the coupling constant and energy, λ_c and E_c , respectively. As above, SSB takes place in the GS solitons at $\lambda < \lambda_c$ or $E > E_c$. We conclude that, while SSB occurs in similar regions for the GS solitons produced with the weak input's asymmetry, the situation is different in the case of the strong initial

asymmetry. For instance, only asymmetric solitons are found at $\lambda < 0.24$ and $E > 2.3$ when $\Delta_{A'}$ is considered. Differently, in the same settings but using $\Delta_{C'}$, the asymmetric states are present at $\lambda < 0.36$ and $E > 1.9$. Therefore, we conclude that, quite naturally, the strong initial asymmetry significantly catalyzes the onset of SSB.

IV. VORTEX SOLITONS

A. Stability

In two-dimensional models with the fractional diffraction, vortices and their stability were studied in many works [72]-[78], [60]. In the present setting, following Ref. [57], the vortex soliton is defined as a set of three solitons in the coupled cores, with phase shifts $2\pi/3$ between them:

$$U_j(t, z) = u_j(t) \exp \left[i \frac{2\pi\sigma}{3} (j-1) + ikz \right], \quad j = 1, 2, 3. \quad (16)$$

The vorticity, with sign (winding number) $\sigma = \pm 1$, is represented by the fact that the total phase gain produced by the round trip comprising the three cores is $\Delta\phi = 2\pi\sigma$, according to ansatz (16).

If functions $u_j(t)$ are real, the substitution of ansatz (16) in Eqs. 5 admits solutions with

$$u_1 = u_2 = u_3 \equiv u(t), \quad (17)$$

satisfying the single real equation:

$$(k - \lambda)u + \frac{1}{2} \left(-\frac{d^2}{dt^2} \right)^{\alpha/2} u - u^3 = 0. \quad (18)$$

Equation (18) is the standard fractional one, which was solved in many works. The solution is characterized by the total energy (6), which reduces to

$$E = \int_{-\infty}^{+\infty} \sum_{j=1,2,3} |u_j(t)|^2 dt \equiv 3 \int_{-\infty}^{+\infty} u^2(t) dt. \quad (19)$$

Our main objective here is to identify a stability area of vortex solitons (16) in the parameter planes of (λ, α) or (E, α) .

To investigate the stability of the vortex modes defined as per Eq. (16) with $\sigma = +1$ (the case of $\sigma = -1$ introduces no difference), the input profile was chosen as the symmetric GS of the decoupled system, i.e., $u_1(t) = u_2(t) = u_3(t) = u^{\text{GS}}(t, \lambda = 0)$.

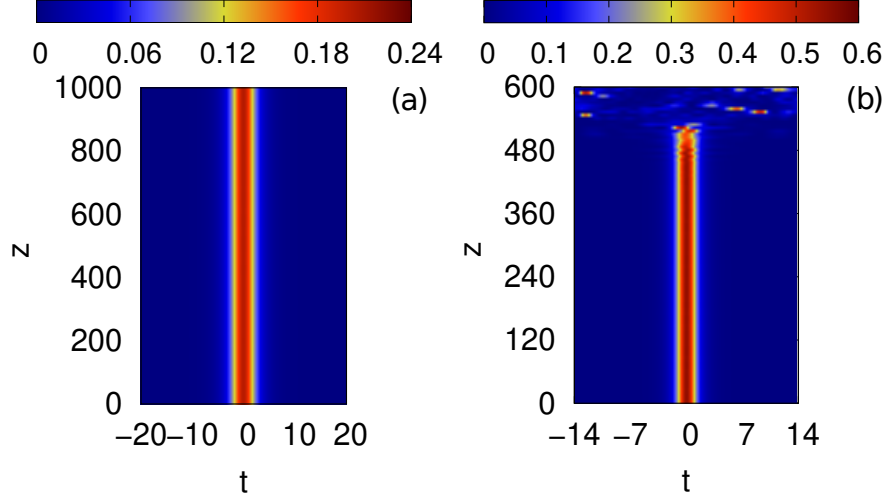


FIG. 11: The evolution of component $|U_3|^2$ of the vortex solitons for $\lambda = 0.3$ and $\alpha = 1.5$.

The total energy of the stable soliton in (a) is $E = 3$, and of the unstable one in (b) is

$$E = 4.2.$$

Numerical simulations show the existence of stable and unstable vortex soliton. Fig. 10(a) presents an example of stable evolution of a vortex soliton with total energy $E = 3$, in the weakly coupled system with $\lambda = 0.1$ and LI $\alpha = 1.2$. The simulations demonstrate stable propagation of this vortex state. It loses stability, following the decrease of the linear-coupling constant λ . In Fig. 10(b), an example of the unstable evolution is displayed, demonstrating the destruction of the vortex soliton (decay into radiation) close to $z = 1050$.

The stability area for the vortex solitons is displayed in Fig. 10(c). It is seen that the stability of the vortex states is favored by low values of LI α . In particular, the vortex modes are stable in the interval of $1 < \alpha < 1.2$.

We also addressed the effect of the total energy of the vortex solitons on their stability. As an example, Fig. 11 demonstrates the evolution of the vortex solitons in the regime of relatively strong coupling ($\lambda = 0.3$), with LI $\alpha = 1.5$, and energies $E = 3$ in (a) and $E = 4.2$ in (b). The simulations demonstrate the stability of the former vortex soliton and instability of the latter one. Further simulations demonstrate that the critical energy, above which the vortex soliton develops the instability, is nearly independent of LI. For example, setting $\lambda = 0.1$, we conclude that the critical energy is $E \approx 3$ in the entire interval of the LI values, $1 < \alpha \leq 2$. Similarly, setting $\lambda = 0.3$, we conclude that the

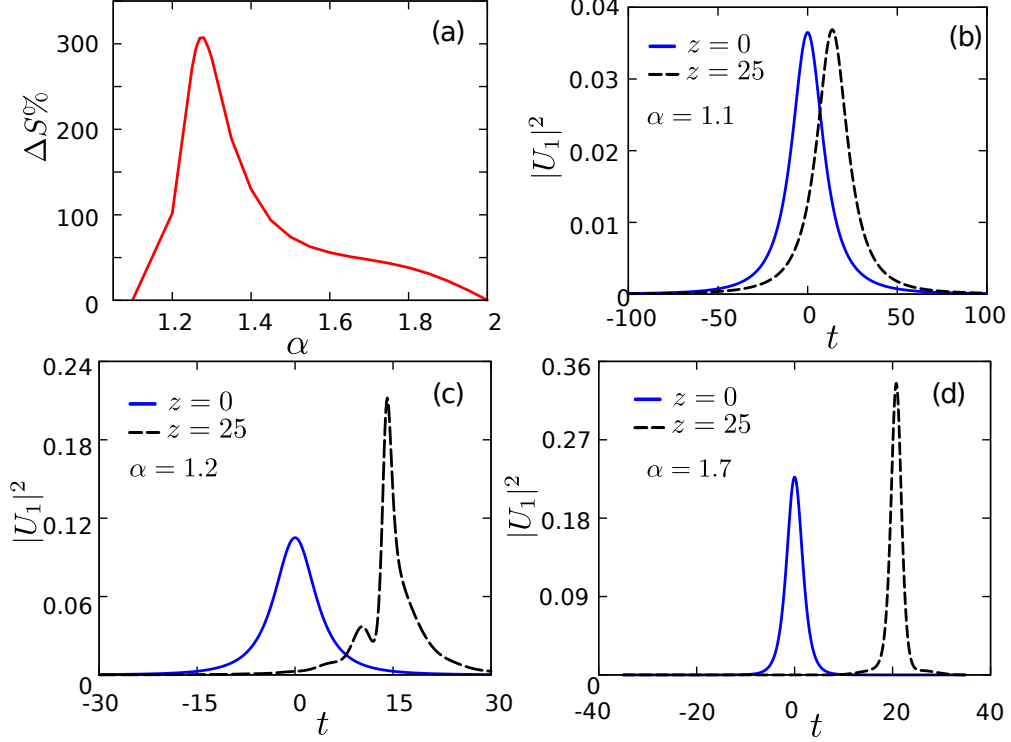


FIG. 12: (a) Relative difference between static and moving vortex (at $z = 25$) mode peaks versus α . Comparison between the vortex modes $|U_1(t, z = 0)|^2$ and $|U_1^b(t, z = 25)|^2$ for $\alpha = 1.1$ (b), $\alpha = 1.2$ (c) and $\alpha = 1.7$ (d).

critical energy, $E \approx 3.3$, again keeps this nearly a constant value in the same interval.

Unlike the GS solitons, the SSB effect was not found in the vortex ones at all values of the parameters for which the analysis was performed in this work. Actually, this fact stresses the exceptional robustness of the vortex solitons, which are protected by their topological charge against the symmetry breaking.

B. Mobility of vortex solitons

The FGVD destroys the usual Galilean invariance of the NLS equation, therefore mobility of fractional solitons is a nontrivial issue [52, 53]. In this work, we address the mobility of vortex solitons, as their internal structure may make them more sensitive to the motion than in the case of the GS solitons considered above.

By means of direct simulations, we studies results of the application of a boost to the

stable vortex soliton,

$$U_j^b(t, z) \rightarrow U_j^b(t, z) = U_j(t, z) \exp(it), \quad (20)$$

with a fixed boost parameter corresponding to $\chi = -1$ in the general expression for the boost factor, $\exp(-i\chi t)$.

The mobility effect is quantified by the relative difference of the peak power between the moving and quiescent (static) vortex solitons,

$$\Delta S = \frac{|\max|U_1^b(t, z)|^2 - \max|U_1(t, z = 0)|^2|}{\max|U_1(t, z = 0)|^2}. \quad (21)$$

Figure 12(a) shows the relative difference (21) as a function of LI α , obtained for a fixed linear-coupling constant, $\lambda = 0.05$. The plot identifies the (relatively low) value of LI, $\alpha = 1.27$, at which the FGVD produce the largest nontrivial effect of the mobility. Although ΔS is small at $\alpha < 1.12$, it is different from zero: for instance, $\Delta S(\alpha = 1.10) = 1.14\%$.

The temporal structures of the quiescent and moving vortex solitons are compared in Figs. 12(a-c). At $\alpha = 1.1$ the boosted vortex soliton moves slowly, featuring a small deformation in the profile. At larger values of LI, such as $\alpha = 1.2$, a large deformation of the vortex is observed, showing partial fragmentation of the temporal profile, initially with a weak peak emerging to the left of the main one. In all cases, changes in moving profiles are independent of the linear-coupling constant λ . This is explained by the fact that the temporal profiles of all the components of the vortex solitons remain identical, as in Eq. (17).

V. CONCLUSION

In the framework of the tri-core optical system combining the intra-core self-focusing and FGVD (fractional group-velocity dispersion), which is modeled by the system of linearly coupled FNLS (fractional nonlinear Schrödinger) equations, we have performed the analysis of GS (ground-state) three-component solitons, and vortex solitons with the triangular (prismatic) structure. For the GS solitons, the SSB (spontaneous-symmetry-breaking) phenomenology is investigated in detail, as the functions of the LI (Lévy index), linear-coupling constant, and total energy of the three-component solitons. The existence diagrams for symmetric and asymmetric GS solitons are plotted, and bifurcation diagrams for SSB are constructed, with the conclusion that the bifurcation is of the

supercritical type. As usual, the SSB is driven by the increase of the nonlinearity and decrease of the linear coupling between the cores. The existence and stability diagrams are produced for vortex solitons too. Unlike the GS solitons, the vortices do not feature SSB. The mobility of the vortex solitons in the fractional medium, imposed by the application of the boost, is studied too.

As an expansion of the work, it may be interesting to study solitons and SSB phenomenology in them, in the framework of a planar, rather than triangular, three-core fractional system. A challenging objective is to develop the FGVD model for nonlinear multi-core systems with the fractional dispersion.

ACKNOWLEDGMENTS

The authors acknowledge the financial support of the Brazilian agencies CNPq (#306105/2022-5) and FAPEG. This work was also performed as part of the Brazilian National Institute of Science and Technology (INCT) for Quantum Information (#465469/2014-0). The work of BAM was supported, in a part, by the Israel Science Foundation through grant No. 1287/17.

-
- [1] V.E. Zakharov, S.V. Manakov, S.P. Novikov, L.P. Pitaevskii, *Theory of Solitons: The Inverse Problem Method* (Nauka Publishers, Moscow, 1980) (English translation: Consultants Bureau, New York, 1984).
 - [2] T. Dauxois, M. Peyrard, *Physics of Solitons* (Cambridge University Press, Cambridge, 2006)
 - [3] G.P. Agrawal, *Nonlinear Fiber Optics* (Elsevier, 2013).
 - [4] Y.S. Kivshar, G.P. Agrawal, *Optical Solitons* (Elsevier, 2003).
 - [5] V.E. Zakharov, *Collapse of Langmuir Waves*, J. Exp. Theor. Phys. **35** (1972) 908.
 - [6] Y.H. Ichikawa, *Topics on solitons in plasmas*, Physica Scripta. **20** (1979) 296-305
 - [7] C.J. Pethick, H. Smith, *Bose–Einstein Condensation in Dilute Gases* (Cambridge University Press, 2008).
 - [8] L.P. Pitaevskii, S. Stringari, *Bose-Einstein Condensation* (Clarendon Press, 2003).

- [9] M. Lakshmanan, *The fascinating world of the Landau–Lifshitz–Gilbert equation: an overview*, Phil. Trans. R. Soc. A **369** (2011) 1280–1300
- [10] N.E. Huang, Z. Shen, S.R. Long, *A new view of nonlinear water waves: The Hilbert spectrum*, Ann. Rev. Fluid Mech. **31** (1999) 417–457
- [11] M.F. Gobbi, J.T. Kirby, G. Wei, *A fully nonlinear Boussinesq model for surface waves*, J. Fluid Mech. **405** (2000) 181–210
- [12] G.A. Maugin, *Nonlinear surface waves and solitons*, Eur. Phys. J. Special Topics, **147** (2007) 209–230
- [13] J. Satsuma, N. Yajima, *Initial value problems of one-dimensional self-modulation of nonlinear waves in dispersive media*, Suppl. Prog. Theor. Phys. **55** (1974) 284–306
- [14] S.M. Jensen, *The nonlinear coherent coupler*, IEEE J. Quantum Electron **18** (1982) 1580–1583
- [15] A.A. Maier, *Optical transistors and bistable devices utilizing nonlinear transmission of light in systems with unidirectional coupled waves*, Sov. J. Quantum Electron **12** (1982) 1490–1494
- [16] M. Romagnoli, S. Trillo, and S. Wabnitz, *Soliton switching in nonlinear couplers*, Opt. Quantum Electron **24** (1992) S1237–S1267
- [17] B.A. Malomed, *A variety of dynamical settings in dual-core nonlinear fibers*, In: *Handbook of Optical Fibers*, Vol. 1, (G.-D. Peng, Editor: Springer, Singapore, 2019) pp. 421–474
- [18] N.N. Akhmediev, A.V. Buryak, *Soliton states and bifurcation phenomena in three-core nonlinear fiber couplers*, J. Opt. Soc. Am. B **11** (1994) 804
- [19] A. Gubeskys, B.A. Malomed, *Solitons in a system of three linearly coupled fiber gratings*, Eur. Phys. J. D **28** (2004) 283–299
- [20] S. Mumtaz, R.J. Essiambre, G.P. Agrawal, *Nonlinear propagation in multimode and multicore fibers: generalization of the Manakov equations*, J. Lightwave Technol. **31** (2013) 398–406
- [21] R.G.H. van Uden, R. Amezcua Correa, E. Antonio Lopez, F.M. Huijskens, C. Xia, G. Li, A. Schülzgen, H. de Waardt, A.M.J. Koonen, C.M. Okonkwo, *Ultra-high-density spatial division multiplexing with a few-mode multicore fibre*, Nature Phot. **8** (2014) 865–870
- [22] I.S. Chekhovskoy, O.V. Shtyrina, S. Wabnitz, M.P. Fedoruk, *Finding spatiotemporal light bullets in multicore and multimode fibers*, Opt. Express **28** (2020) 7817–7828
- [23] L.G. Wright, F.O. Wu, D.N. Christodoulides, F.W. Wise, *Physics of highly multimode nonlinear optical systems*, Nature Phys. **18** (2022) 1018–1030

- [24] V.H. Nguyen, L.X.T. Tai, I. Bugar, M. Longobucco, R. Buzcynski, B.A. Malomed, M. Trippenbach, *Reversible ultrafast soliton switching in dual-core highly nonlinear optical fibers*, Opt. Lett. **45** (2020) 5221-5224
- [25] T. Mayteevarunyoo, B.A. Malomed, G. Dong, *Spontaneous symmetry breaking in a nonlinear double-well structure*, Phys. Rev. A **78** (2008) 53601
- [26] S. Kumar, P. Li, L. Zeng, J. He, B.A. Malomed, *A solvable model for symmetry-breaking phase transitions*, Sci. Rep. **13**(2023) 13768
- [27] A. Acus, B.A. Malomed, Y. Shnir, *Spontaneous symmetry breaking of binary fields in a nonlinear double-well structure*, Physica D **241** (2012) 987
- [28] N. Laskin, *Fractional quantum mechanics and Lévy path integrals*, Phys. Lett. A **268** (2000) 298
- [29] N. Laskin, *Fractional Schrödinger equation*, Phys. Rev. E **66** (2002) 56108
- [30] X. Guo, M. Xu, *Some physical applications of fractional Schrödinger equation*, J. Math. Phys. **47** (2006) 082104
- [31] N. Laskin, *Fractional Quantum Mechanics* (World Scientific, Singapore, 2018).
- [32] S. Longhi, *Fractional Schrödinger equation in optics*, Opt. Lett. **40** (2015) 1117
- [33] S. Liu, Y. Zhang, B.A. Malomed, E. Karimi, *Experimental realisations of the fractional Schrödinger equation in the temporal domain*, Nature Comm. **14** (2023) 222
- [34] L. Zhang, Z. He, C. Conti, Z. Wang, Y. Hu, D. Lei, Y. Li, and D. Fan, *Modulational instability in fractional nonlinear Schrödinger equation*, Commun. Nonlinear Sci. Numer. Simul. **48** (2017) 531
- [35] W.-P. Zhong, M.R. Belić, B.A. Malomed, Y. Zhang, T. Huang, *Spatiotemporal accessible solitons in fractional dimensions*, Phys. Rev. E **94** (2016) 012216
- [36] W.-P. Zhong, M. Belić, Y. Zhang, *Accessible solitons of fractional dimension*, Ann. Phys. (N. Y). **368** (2016) 110
- [37] S. Secchi, M. Squassina, *Soliton dynamics for fractional Schrödinger equations*, Appl. Anal. **93** (2014) 1702
- [38] Y. Hong, Y. Sire, *A new class of traveling solitons for cubic fractional nonlinear Schrödinger equations*, Nonlinearity **30** (2017) 1262
- [39] M. Chen, S. Zeng, D. Lu, W. Hu, Q. Guo, *Optical solitons, self-focusing, and wave collapse in a space-fractional Schrödinger equation with a Kerr-type nonlinearity*, Phys. Rev. E **98** (2018) 022211

- [40] Q. Wang, J. Li, L. Zhang, W. Xie, *Hermite-gaussian-like soliton in the nonlocal nonlinear fractional Schrödinger equation*, EPL **122** (2018) 64001
- [41] H. Sakaguchi, B.A. Malomed, *Two-dimensional solitons in second-harmonic-generating media with fractional diffraction*, Physica D **467** (2024) 134242
- [42] C. Huang, L. Dong, *Gap solitons in the nonlinear fractional Schrödinger equation with an optical lattice*, Opt. Lett. **41** (2016) 5636
- [43] J. Xiao, Z. Tian, C. Huang, L. Dong, *Surface gap solitons in a nonlinear fractional Schrödinger equation*, Opt. Express **26** (2018) 2650
- [44] P. Li, B.A. Malomed, D. Mihalache, *Metastable soliton necklaces supported by fractional diffraction and competing nonlinearities*, Opt. Express **28** (2020) 34472
- [45] Y. Qiu, B.A. Malomed, D. Mihalache, X. Zhu, X. Peng, Y. He, *Stabilization of single-and multi-peak solitons in the fractional nonlinear Schrödinger equation with a trapping potential*, Chaos, Solitons & Fractals **140** (2020) 110222
- [46] L. Zeng, D. Mihalache, B.A. Malomed, X. Lu, Y. Cai, Q. Zhu, J. Li, *Families of fundamental and multipole solitons in a cubic-quintic nonlinear lattice in fractional dimension*, Chaos, Solitons & Fractals **144** (2021) 110589
- [47] L. Zeng, J. Zeng, *Families of fundamental and multipole solitons in a cubic-quintic nonlinear lattice in fractional dimension*, Opt. Lett. **44** (2019) 2661
- [48] M.C.P. dos Santos, B.A. Malomed, W.B. Cardoso, *Solitons supported by a self-defocusing trap in a fractional-diffraction waveguide*, Chin. J. Phys. **89** (2024) 1474-1482
- [49] L. Zeng, J. Zeng, *Preventing critical collapse of higher-order solitons by tailoring unconventional optical diffraction and nonlinearities*, Commun. Phys. **3** (2020) 26
- [50] Q. Wang, G. Liang, *Vortex and cluster solitons in nonlocal nonlinear fractional Schrödinger equation*, J. Optics **22**(2020) 055501
- [51] P. Li, B.A. Malomed, D. Mihalache, *Vortex solitons in fractional nonlinear Schrödinger equation with the cubic-quintic nonlinearity*, Chaos, Solitons & Fractals **137** (2020) 109783
- [52] B.A. Malomed, *Optical solitons and vortices in fractional media: a mini-review of recent results*, Photonics **8** (2021) 353
- [53] B.A. Malomed, *Basic fractional nonlinear-wave models and solitons, Optical solitons and vortices in fractional media: A mini-review of recent results*, Chaos **34** (2024) 022102
- [54] L. Zeng, J. Zeng, *Fractional quantum couplers*, Chaos, Solitons & Fractals **140** (2020) 110271

- [55] L. Zeng, J. Shi, X. Lu, Y. Cai, Q. Zhu, H. Chen, H. Long, J. Li, *Stable and oscillating solitons of \mathcal{PT} -symmetric couplers with gain and loss in fractional dimension*, *Nonlinear Dyn.* **103** (2021) 1831
- [56] D.V. Strunin, B. A. Malomed, *Symmetry-breaking transitions in quiescent and moving solitons in fractional couplers*, *Phys. Rev. E* **107** (2023) 064203
- [57] A. Sigler, B.A. Malomed, D.V. Skryabin, *Localized states in a triangular set of linearly coupled complex Ginzburg-Landau equations*, *Phys. Rev. E* **74** (2006) 066604
- [58] M. Cai, C.P. Li, *On Riesz derivative*, *Fract. Calc. Appl. Anal.* **22** (2019) 287–301
- [59] B.B. Mandelbrot, *The Fractal Geometry of Nature* (W. H. Freeman, New York, 1982).
- [60] H. Sakaguchi, B. A. Malomed, *One- and two-dimensional solitons in spin-orbit-coupled Bose-Einstein condensates with fractional kinetic energy*, *J. Phys. B: At. Mol. Opt. Phys.* **55** (2022) 155301
- [61] J. Chen, J. Zeng, *Spontaneous symmetry breaking in purely nonlinear fractional systems*, *Chaos* **30** (2020) 063131
- [62] L. Salasnich, B.A. Malomed, *Spontaneous symmetry breaking in linearly coupled disk-shaped Bose-Einstein condensates*, *Mol. Phys.* **109** (2011) 2737-2745
- [63] S. Duo, Y. Zhang, *Mass-conservative Fourier spectral methods for solving the fractional nonlinear Schrödinger equation*, *Comput. Math. with Appl.* **71** (2016) 2257
- [64] M. Jeng, S.-L.-Y. Xu, E. Hawkins, J.M. Schwarz, *On the nonlocality of the fractional Schrödinger equation*, *J. Math. Phys.* **51** (2010) 62102
- [65] Y. Luchko, *Fractional Schrödinger equation for a particle moving in a potential well*, *J. Math. Phys.* **54** (2013) 12111
- [66] J. Yang, *Nonlinear Waves in Integrable and Nonintegrable Systems* (SIAM, Philadelphia, 2010).
- [67] W.Z. Bao, Q. Du, *Computing the ground state solution of Bose-Einstein condensates by a normalized gradient flow*, *SIAM J. Sci. Comp.* **25** (2004) 1674-1697
- [68] M.C.P. dos Santos, W. B. Cardoso, *Localization of light waves in self-defocusing fractional systems confined by a random potential*, *Nonlinear Dyn.* **112** (2024) 2209-2217
- [69] G. Mazzarella, L. Salasnich, *Spontaneous symmetry breaking and collapse in bosonic Josephson junctions*, *Phys. Rev. A* **82** (2010) 33611
- [70] B.M. Miranda, M.C.P. dos Santos, W.B. Cardoso, *Symmetry breaking in Bose-Einstein condensates confined by a funnel potential*, *Phys. Lett. A* **452** (2022) 128453

- [71] G. Iooss, D.D. Joseph, *Elementary Stability Bifurcation Theory* (Springer-Verlag, New York, 1980).
- [72] X. Yao, X. Liu, *Off-site and on-site vortex solitons in space-fractional photonic lattices*, *Opt. Lett.* **43** (2018) 5749–5752
- [73] Z. Wu, P. Li, Y. Zhang, H. Guo, Y. Gu, *Multicharged vortex induced in fractional Schrödinger equation with competing nonlocal nonlinearities*, *J. Optics* **21** (2019) 105602
- [74] L. Dong, C. Huang, *Vortex solitons in fractional systems with partially parity-time-symmetric azimuthal potentials*, *Nonlinear Dyn.* **98** (2019) 1019–1028
- [75] Q. Wang, G. Liang, *Vortex and cluster solitons in nonlocal nonlinear fractional Schrödinger equation*, *J. Optics* **22** (2020) 055501
- [76] P. Li, B.A. Malomed, D. Mihalache, *Metastable soliton necklaces supported by fractional diffraction and competing nonlinearities*, *Opt. Exp.* **28** (2020) 34472–33488
- [77] S. He, B.A. Malomed, D. Mihalache, X. Peng, X. Yu, Y. He, D. Den, *Propagation dynamics of abruptly autofocusing circular Airy Gaussian vortex beams in the fractional Schrödinger equation*, *Chaos, Solitons & Fractals* **142** (2021) 110470
- [78] S. He, B.A. Malomed, D. Mihalache, X. Peng, Y. He, D. Deng, *Propagation dynamics of radially polarized symmetric Airy beams in the fractional Schrödinger equation*, *Phys. Lett. A* **404** (2021) 127403
- [79] M. Zhong, *Two-dimensional fractional PPT-symmetric cubic-quintic NLS equation: Double-loop symmetry breaking bifurcations, ghost states and dynamics*, *Physica D* **448** (2023) 133727
- [80] M. Zhong, L. Wang, P. Li, Z. Yan, *Spontaneous symmetry breaking and ghost states supported by the fractional PT-symmetric saturable nonlinear Schrödinger equation*, *Chaos* **33** (2023) 013106